European Electricity Grids May Exhibit Heatwave-induced Capacity Bottlenecks

Enming Liang[1], Minghua Chen[1,2*], Srinivasan Keshav[3*]

[1]Department of Data Science, City University of Hong Kong.
[2]School of Data Science, The Chinese University of Hong Kong (Shenzhen).
[3]Department of Computer Science and Technology, University of Cambridge.

*Corresponding author(s). E-mail(s): minghua.chen@cityu.edu.hk; sk818@cam.ac.uk;
Contributing authors: eliang4-c@my.cityu.edu.hk;

As climate change increases the frequency, intensity, and duration of heatwaves, understanding their impact on electricity grids is crucial for enhancing societal security and resilience. We study the effects of heatwaves on European electricity grids using several comprehensive real-world datasets. Moreover, noting that conventional modeling of temperature effects on grid operation limits is insufficient or computationally challenging, we develop a novel temperature-dependent modeling framework that is both comprehensive and efficient. We apply this method to evaluate the robustness of several European electricity grids for projected heatwave scenarios for the next 5 years. We identify concerning grid bottlenecks and substantial national differences in vulnerability: for example, while the Spanish grid exhibits temperature-induced capacity bottlenecks that could jeopardize power supply during heatwaves, the German grid shows remarkable resilience. These findings emphasize the need for temperature-aware grid power flow analysis as well as the need for long-range planning to ensure energy security despite climate-change induced future heatwaves.

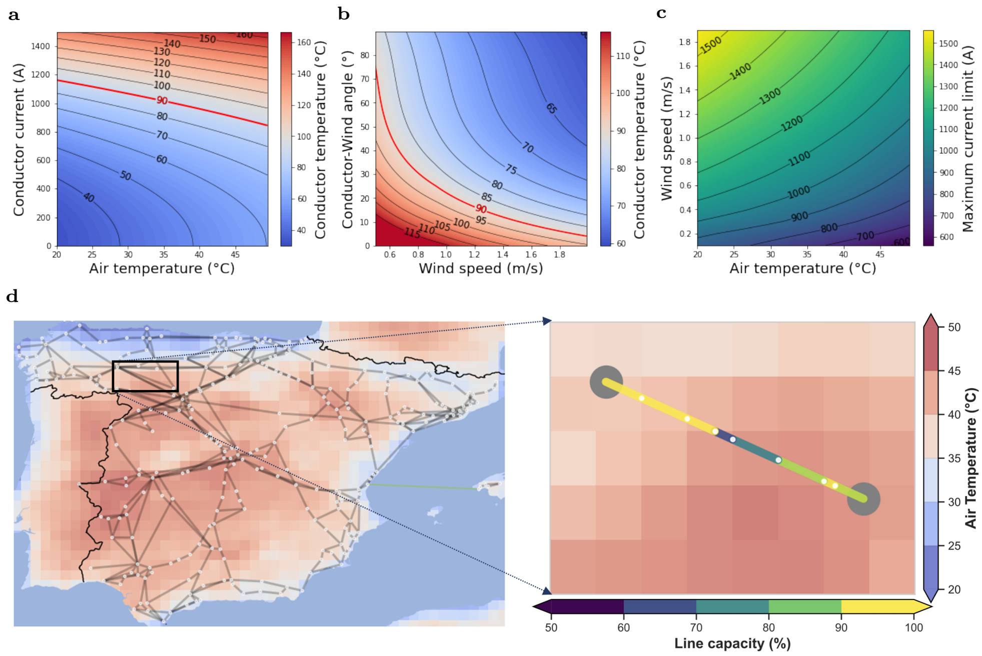

Fig. 1: **Heatwaves reduce current capacity and induce transmission line bottlenecks**. **a-c** Physical properties of conductors based on IEEE Std 738$^{\mathrm{TM}}$-2012 under varying weather conditions [1]. **a** Conductor temperature as a function of air temperature and line current. **b** Conductor temperature variations with different wind speeds and angles. **c** Line current capacity under different air temperatures and wind speeds. **d** Line segment capacity variations along a 130-km transmission line in Northwestern Spain crossing 9 gridded regions, showing localized thermal constraints compared to nominal capacity during heatwaves.

Introduction

Climate change has led to an increase in average global temperatures, characterized by more frequent, intense, and prolonged heatwaves [2–5]. The escalating frequency and severity of heatwaves impact millions of people worldwide [6–8] and pose significant challenges to critical infrastructure [9, 10], including electrical power grids [11, 12]. A detailed understanding of these impacts on power grid performance is crucial for evaluating and enhancing societal resilience and energy security.

Heatwaves create a triple threat to electrical grids. First, they substantially increase cooling demand, driving up electricity consumption [4]. Second, they alter power generation capacity through mechanisms such as wind energy shortages [13] and generator capacity derating [14]. Third, they reduce transmission line capacity as conductors approach their thermal limits (see Fig. 1a-c). Moreover, regional variations in weather conditions create spatially heterogeneous thermal constraints along long-distance transmission lines, with different segments experiencing different capacity reductions (Fig. 1d).

Traditional power flow analyses inadequately capture these heatwave impacts. Existing linearized optimal power flow (OPF) models, even those incorporating weather-dependent dynamic line ratings [15], fail to represent the complex grid dynamics that emerge under heavy cooling loads during extreme heat. More critically, they do not precisely model temperature effects on generator capacity derating and the segment-specific thermal constraints of long transmission lines [16]. This oversight leads to incomplete vulnerability assessments, as our European case studies demonstrate.

We address these methodological limitations through a novel framework that combines comprehensive heatwave-aware grid modeling approaches (Fig. 2a) with an efficient temperature-dependent alternating-current (AC) OPF analysis under future heatwave projections (Fig. 2b). Our approach introduces four key innovations: (i) temperature-dependent electricity demand estimation and generation derating modeling, (ii) per-segment conductor heat balance modeling to determine thermal-dependent capacity limits for transmission lines, (iii) probabilistic assessment using hundreds of bias-corrected heatwave projections with geospatially-gridded weather profiles, and (iv) an efficient iterative algorithm for temperature-dependent OPF analysis that enables rapid evaluation of national grid resilience across these numerous scenarios. Applying our framework to European electricity grids using publicly available weather profiles, power demand models, renewable penetration scenarios, and grid parameters, we reveal:

▷ We demonstrate that existing grid resilience analyses based on standard AC-OPF approaches fail to adequately capture the combined effects of increased cooling demand and reduced transmission capacity during heatwaves. Even more accurate quadratic approximations for thermal constraints [17] still substantially underestimate transmission line vulnerabilities under extreme heat.

▷ We formulate a temperature-dependent AC-OPF problem that simultaneously incorporates temperature-dependent cooling loads, generator derating, and segment-specific thermally-induced capacity limits for transmission lines, using hundreds of heatwave projections with weather profiles at approximately 30km resolution. We develop a novel iterative algorithm that solves this OPF problem more efficiently while capturing critical nonlinear interactions missed by existing methods.

▷ Applying our framework to European grids reveals significant heatwave vulnerability. For example, by 2029, up to 5.5% of Spanish transmission lines are projected to drop below 70% of their nominal current-carrying capacity—a typical security constraint margin [18], highlighting the need for heatwave-aware grid management. National-level impacts vary dramatically: the Spanish grid faces substantial load shedding risk under extreme heat, while the German grid demonstrates remarkable resilience. While these findings are based on the best available public data, we caution that further validation with proprietary grid-specific datasets would strengthen these estimations.

These findings underscore the urgent need for grid operators and policymakers to consider the impacts of extreme weather more comprehensively in their planning and management strategies. By doing so, they can enhance the reliability and resilience of electricity supplies in the face of increasing climate change challenges.

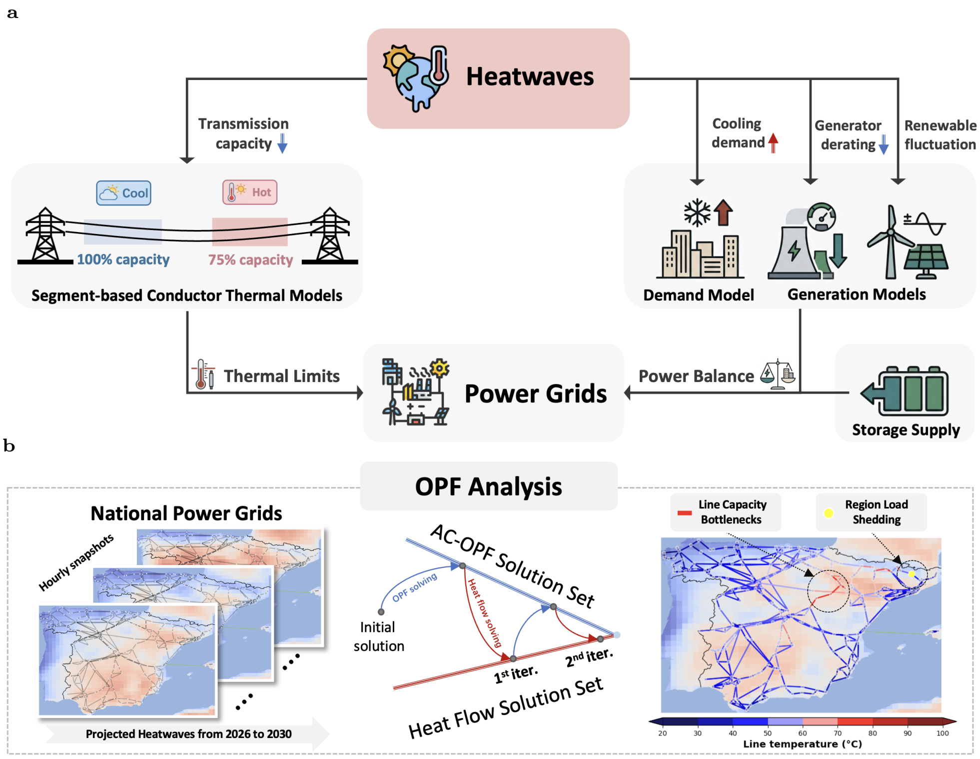

Fig. 2: **Framework for analyzing heatwave impacts on national power grids. a** Integration of segment-specific conductor thermal modeling, temperature-dependent demand, weather-dependent renewable generation, and heatwave-induced generation derating to capture climate-power system interactions. **b** Proposed iterative algorithm solving temperature-dependent AC optimal power flow under bias-corrected heatwave projections, identifying capacity bottlenecks and potential load shedding regions during extreme heat events.

Results

Setup

We employ the modeling framework illustrated in Fig. 2**a**, with data sources and detailed methods included in Section 1, to evaluate how heatwaves impact existing grid operations in European countries under projected future heatwave scenarios. We focus our analysis on 2026–2030, a time horizon that reduces uncertainty in both climate projections and grid infrastructure configurations while providing actionable insights for near-term resilience planning and investment decisions. We conduct optimal power flow (OPF) analyses under projected heatwave scenarios, using the proposed iterative algorithms in Fig. 2**b**, to investigate whether national grids exhibit temperature-induced capacity bottlenecks, indicated by transmission lines approaching their thermal limits and load-shedding regions—that is, buses where power

a

Year	**Wind** (m/s)	**Solar** (W/m^2)	**Temp.** (℃)	**Load** (GWh)
2026	2.27 (±0.37)	785.52 (±67.23)	36.05 (±2.59)	36.47 (±1.45)
2027	2.87 (±0.36)	753.82 (±70.45)	36.92 (±2.58)	37.48 (±1.33)
2028	2.65 (±0.40)	717.83 (±91.25)	36.93 (±3.46)	37.98 (±2.12)
2029	2.62 (±0.43)	789.08 (±66.75)	37.52 (±2.58)	38.23 (±1.36)
2030	2.69 (±0.35)	766.68 (±62.69)	37.58 (±2.58)	38.71 (±1.62)

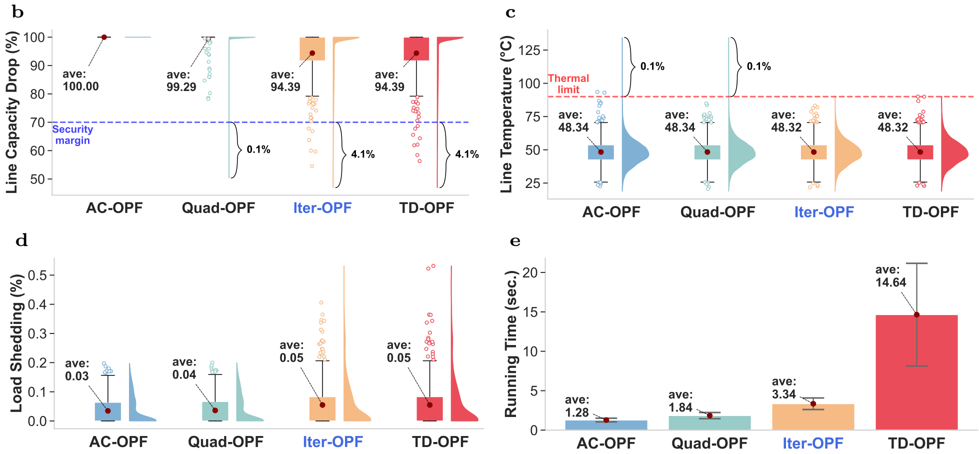

Fig. 3: **Comparison of different OPF methods for analyzing the Spanish grid under projected heatwaves.** We compare basic AC-OPF, advanced Quad-OPF, our proposed Iter-OPF, and the most accurate TD-OPF. **a** Weather and load statistics under heatwave projections from 2026 to 2030, with **480** hourly scenarios generated in total using a bias-correction approach (detailed in Section 1.1). **b–c** Distributions of estimated line capacity reduction compared to nominal conditions and line temperatures (derived from heat balance equations) across different methods. Average values and percentages above/below thresholds are indicated. **d** Distributions of load shedding ratios (demand-generation mismatch over total demand). **e** Average per-scenario solving times.

injection fails to meet consumption. Our work compares the accuracy of existing OPF analysis methods with our proposed approach in identifying these critical bottlenecks while satisfying physical constraints. Detailed setups are in Sec. 1 and Supplementary Section 3. Complete simulation results are in Supplementary Section 4.

Observations

We find that, as heatwaves simultaneously reduce transmission capacity, cause generator derating, and increase cooling demand, some European national grids, such as Spain, France, and Italy, exhibit capacity bottlenecks in projected heatwave scenarios, subsequently resulting in non-negligible load-shedding. Unmet cooling demand during heatwaves can lead to potential human casualties [19, 20] This alerting observation emphasizes the need for temperature-aware grid analysis and planning to mitigate heatwave risks and ensure energy security. In detail, we have the following observations.

Existing OPF models overestimate grid resilience under heatwaves

We compare four OPF-based approaches: the standard alternating current OPF (AC-OPF), a more advanced ACOPF with quadratic approximation of thermal limits (Quad-OPF), our proposed iterative framework (Iter-OPF), and the most accurate fully converged temperature-dependent ACOPF (TD-OPF). Detailed formulations are in Section 1.5 and Supplementary Section 2.

Conventional methods substantially underestimate heatwave risks. AC-OPF neglects thermal limits entirely, while Quad-OPF's quadratic approximation fails to precisely capture the complex nonlinear relationship between temperature and current-carrying capacity (Fig. 3b). Both methods permit line temperatures to exceed the 90°C thermal limit (Fig. 3c), overestimating transmission capacity and underestimating load shedding (Fig. 3d). Implementing generation plans based on these methods during heatwaves could trigger line shutdowns or even cascading blackouts [21, 22].

Our Iter-OPF framework addresses these limitations. Like TD-OPF, it correctly identifies load shedding regions and maintains safe line temperatures below 90°C. Yet while TD-OPF requires over four times the computational cost of AC-OPF (Fig. 3e), Iter-OPF achieves comparable accuracy at only twice the cost, enabling reliable resilience assessment across hundreds of weather scenarios for comprehensive grid planning.

Complete thermal modeling is essential for accurate resilience assessment under heatwaves

To assess the importance of different modeling components under heatwaves, we conduct an ablation study systematically removing key elements from Iter-OPF: conductor thermal models, segment-based modeling, and generator derating (Fig. 4a–b). We also compare these against the widely used 70% security margin SC-OPF approach [18].

Conductor thermal modeling proves most critical. Removing it substantially overestimates grid capacity, while segment-based modeling captures local thermal bottlenecks that uniform approaches miss (Fig. 4a). Generator derating has comparatively smaller impacts on system-level performance.

The 70% security margin approach [18], though commonly used, only partially prevents line overheating (Fig. 4b). This fixed margin cannot avoid thermal violations because it neglects spatial heterogeneity in thermal conditions—actual capacity can drop near 50% of nominal ratings during extreme heatwaves in localized hotspots (Fig. 3d). These results demonstrate that explicit temperature-dependent thermal modeling is essential; conservative static margins alone are insufficient for reliable heatwave resilience assessment.

Rising demand amplifies grid stress, yet energy storage alone offers limited relief

We assess grid resilience sensitivity to future demand growth and energy storage availability. With load growth rates from 1% to 3% annually from 2025, reflecting emerging demands from AI infrastructure, electrified heating and cooling, and electric

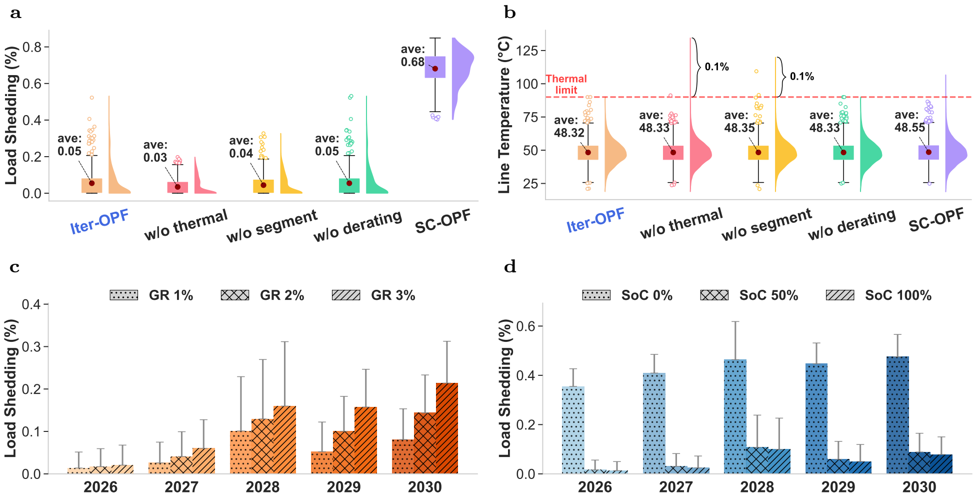

Fig. 4: **Sensitivity analysis of modeling components and environmental factors on OPF analysis under heatwaves. a–b** Impact of removing different modeling components from the Iter-OPF framework on load shedding ratios and line temperatures, compared to the 70% security margin SC-OPF method [18]. **c–d** Load shedding ratios under different load growth rates (GR) and energy storage states (i.e., SoC).

---

vehicles [23, 24], load shedding increases proportionally with demand (Fig. 4c). This positive relationship reveals that rising consumption patterns will directly amplify grid stress during heatwaves.

On the other hand, varying energy storage state-of-charge (SoC) from 0% to 100% yields only marginal reductions in load shedding (Fig. 4d). This counterintuitive result arises because transmission constraints—not generation capacity—dominate grid vulnerability during extreme heat. Higher storage availability cannot compensate when reduced line capacity prevents power delivery from storage units to demand centers. This finding indicates that expanding the capacity of existing storage infrastructure alone cannot adequately mitigate heatwave impacts. Planning must combine transmission upgrades and distributed flexibility to address thermal constraints directly.

Grid vulnerability differs by country and cross-border ties are not always helpful

Grid vulnerability to heatwaves varies dramatically across eight Western European countries. The French electricity grid shows severe thermal-induced capacity bottlenecks during extreme heat, with average load shedding reaching 0.45% and standard deviation of about 1.27% under projected heatwaves (Fig. 5a), leading to potential human casualties [19, 20]. In contrast, Germany, the UK, and other northern countries maintain full supply without load shedding under the same projected scenarios (Fig. 5b).

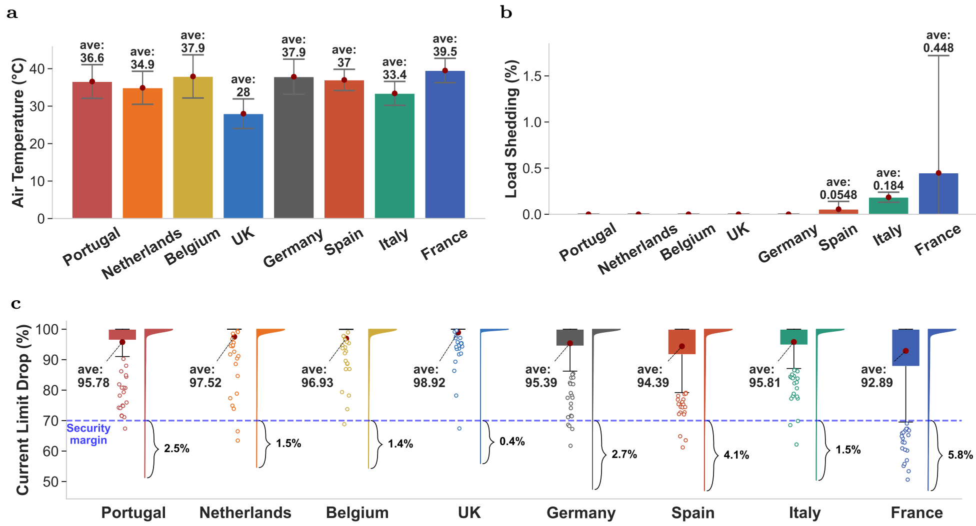

Fig. 5: **National grids in Western Europe, such as France, Italy, and Spain, exhibit substantial load shedding under projected heatwaves, while other countries remain resilient. a** Average air temperature during the hottest hours in projected heatwave periods. **b** Average load shedding across different countries. **c** Distribution of line capacity reduction compared to nominal ratings during heatwaves.

Cross-border interconnections provide asymmetric benefits depending on neighboring grid conditions. France experiences substantial relief from power sharing with less-stressed neighbors—load shedding decreases by about 1.38% when interconnected with Italy (Fig. 6b,d). Conversely, joint simulations of Spain with Portugal or France show minimal relief because France faces similar thermal stress during concurrent heatwaves and also because limited transmission capacity constrains power delivery to stress centers (Fig. 6a,c). This disparity arises because interconnection effectiveness depends on the spatial correlation of climate stress, available surplus capacity in neighboring systems, and sufficient transmission infrastructure to deliver power where needed.

These findings highlight that climate-resilient grid planning requires coordinated European strategies. Countries facing severe thermal constraints need targeted infrastructure upgrades—particularly transmission capacity and cooling systems—while strategic interconnections can provide mutual support where climate impacts are spatially decorrelated.

Broader Implication

Our findings have immediate implications for European energy policy. Grid operators should periodically re-evaluate resilience assessments using temperature-dependent methodologies and the latest climate projections. Policymakers should combine transmission upgrades in thermally vulnerable corridors—particularly in southern Europe—rather than relying solely on storage expansion or demand response. The

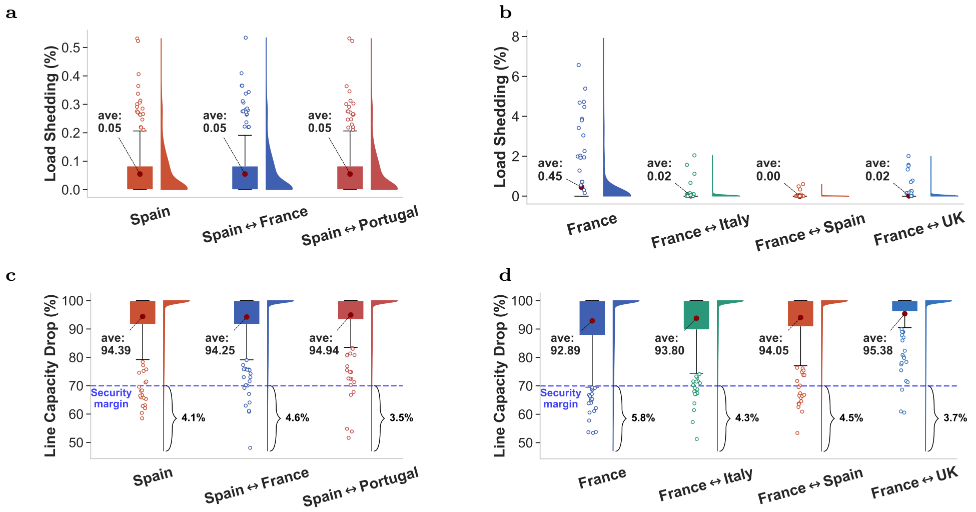

Fig. 6: **Cross-border interconnections enhance grid resilience by enabling mutual support during heatwaves.** We compare single-country analyses with joint multi-country analyses under identical heatwave projections to quantify the effects of cross-border interconnections on grid resilience. **a**–**b** Distribution of Load shedding ratio in Spain and France across different interconnection scenarios. **c**–**d** Distribution of Line capacity reduction in Spain and France across different interconnection scenarios.

---

spatial correlation of climate stress across borders further underscores the need for pan-European coordination; interconnection benefits depend critically on whether neighboring systems face concurrent thermal constraints.

Limitations

Whilst concerning, we note that our results rely on publicly available datasets for European grids, which lack the granular detail accessible to grid operators. Additionally, although we use the best currently available locally bias-corrected weather projections [25], these remain subject to revision as climate models improve. Similarly, projecting cooling load patterns involves inherent uncertainties stemming from evolving building efficiency standards, air conditioning adoption rates, and demand response capabilities.

We focus on near-term scenarios (2026–2030) to reduce forecasting uncertainty; longer-term climate impacts and grid vulnerabilities may be more severe. However, future grid evolution—including increased renewable energy penetration, transmission capacity upgrades, energy storage deployment, and demand increasing—remains uncertain and could substantially alter these vulnerability projections [26]. Our analysis, therefore, represents current grid configurations under near-term climate scenarios rather than a long-term forecast of grid performance.

Our iterative algorithm has been validated against the fully converged TD-OPF model, demonstrating numerical consistency with the underlying physical models. However, the TD-OPF model itself has not been validated against real-world field tests of line temperatures during heatwave events. Errors in the underlying physical model or biased input data will propagate through our analysis.

Given these limitations, grid operators should validate our findings against historical outage records and apply our methodology with their proprietary, higher-resolution models and real-time operational data for more precise vulnerability assessments.

Discussion and Conclusion

Extreme heat poses a compound threat to electrical grids—simultaneously increasing cooling demand, reducing generation efficiency, and degrading transmission capacity. Yet existing assessment methods fail to capture these coupled dynamics or provide the computational efficiency needed for probabilistic analysis across numerous climate scenarios. Current models also overlook the spatially heterogeneous, weather-dependent thermal limits along individual transmission line segments.

We address these gaps with a framework integrating thermal modeling across demand, generation, and transmission with geospatially-gridded climate projections. Our iterative algorithm efficiently solves the temperature-dependent optimal power flow problem while incorporating segment-specific thermal limits, capturing critical nonlinear interactions that existing methods miss. Applying this framework to Western European grids reveals substantial variation in national resilience: Germany's grid can withstand projected extreme heat, while Spain and France face significant vulnerability to supply disruptions.

The heatwave-induced capacity bottlenecks identified by our work can be mitigated through three complementary approaches. First, demand response programs in affected load centers can maintain grid integrity, though at the cost of consumer inconvenience. Second, reconductoring vulnerable transmission lines—which our analysis specifically identifies—can increase capacity and resilience, though this requires capital investment and significant lead time. Third, deploying grid-scale storage at bottleneck locations could compensate for transmission limits during extreme heat events, an approach that warrants investigation as storage costs continue to decline.

Climate change is accelerating while grid infrastructure evolves slowly. The methods and findings presented here provide a foundation for prioritizing adaptation investments before the next extreme heatwave tests grid limits. Future work should extend our framework to optimize adaptation investments under climate uncertainty, incorporating cost-benefit analysis and long-term climate trajectories. Our analysis relies on diverse datasets, not all of which are easy to obtain or process, such as country-specific calibrated demand models. To support reproducibility and enable broader application, we openly share our datasets, algorithms, and source code.

1 Methods

Data Sources

We employed multiple publicly available datasets covering European transmission infrastructure, climate conditions, power demand, and renewable generation. The European transmission network topology and parameters were derived from PyPSA-Eur [18, 27], an open-source model of the European energy system. Algorithm validation used standardized IEEE power flow benchmarks from PGLIB [28]. Historical climate data were obtained from ERA5 [29], providing hourly meteorological fields at $0.25^{\circ} \times 0.25^{\circ}$ resolution from 1940 to present. Future climate projections were sourced from the Copernicus Climate Change Service Energy dataset [30], covering 2005–2100 with temperature, solar irradiance, and wind velocity fields. Historical electricity demand profiles were extracted from ENTSO-E Power Statistics [31]. Weather-dependent demand variations were modeled following Demand.ninja [32]. Renewable generation potentials and time series were computed using Atlite [33].

Comprehensive dataset descriptions are provided in Supplementary Table 1.

Models and Algorithms

We developed a comprehensive framework to assess transmission grid resilience under extreme heatwaves, integrating heatwave projection, demand modeling, and optimal power flow analysis. As depicted in Fig. 2, the framework comprises:

- **Future Heatwave Projection (Sec. 1.1):** Generates multiple projected heatwave events for 2025–2030 based on historical events from 2019, 2022, and 2024.
- **Future Demand Modeling (Sec. 1.2):** Simulates power demand under varying annual growth rates using a weather-dependent model from Demand.ninja [32].
- **Generator Derating Modeling (Sec. 1.3):** Quantifies reduced generator efficiency due to elevated ambient temperatures during heatwaves.
- **Renewable Generation:** Calculates renewable generation potential under projected weather conditions using Atlite [33].
- **Transmission Line Thermal Modeling (Sec. 1.4):** Quantifies temperature effects on conductor properties and thermal limits, including multi-bundle line derating and segmented analysis to identify localized stress points.
- **Optimal Power Flow Analysis (Sec. 1.5):** Integrates these components to simulate grid response under thermal and demand stresses, revealing critical capacity constraints and vulnerability zones.

1.1 Future Heatwave Modeling

We adopt future reference climate variables based on the bias-corrected European regional climate model, CORDEX, under the RCP 4.5 scenario for the European domain [30]. However, these reference climate data are averaged over three-hour intervals and lack prediction uncertainty intervals, thus inadequately capturing shorter-duration extreme heat events.

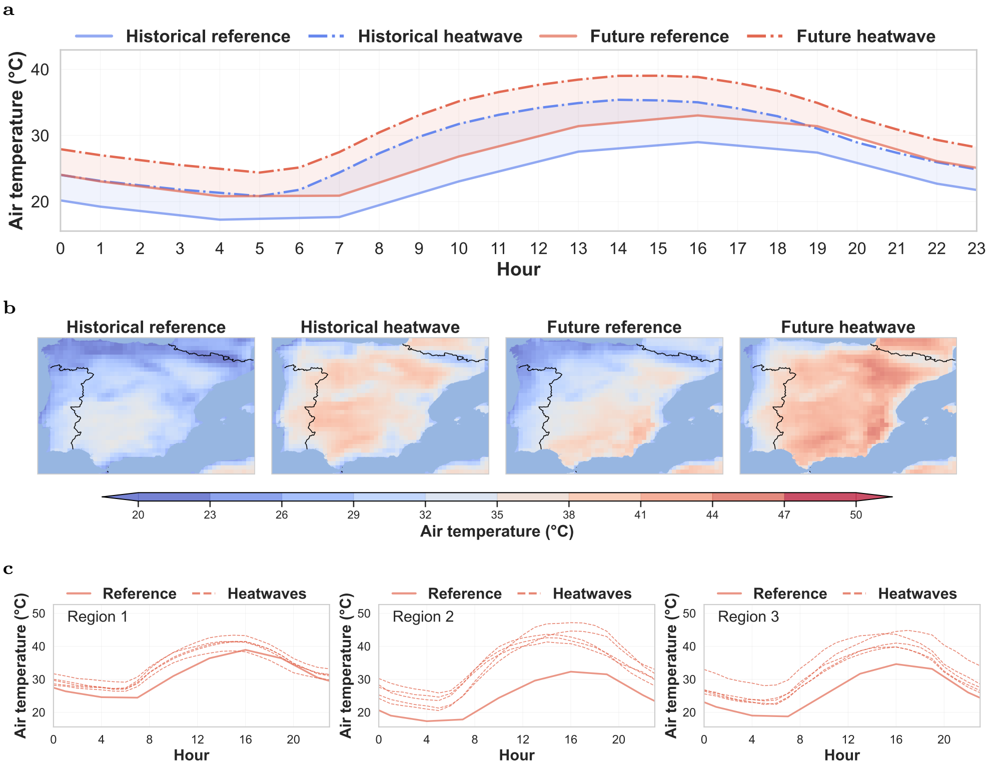

Fig. 7: **Projected 2030 heatwaves in Spain derived from 2022 observations. a** Morphing approach for projecting future heatwaves. Delta values calculated from a historical heatwave day are applied to a future reference day to generate projected conditions. Temperature values represent spatial averages across regions. **b** Spatial characteristics of generated heatwaves compared to historical events and reference profiles. The morphing approach preserves spatial and temporal patterns from historical events. **c** Generated 2030 heatwaves based on delta values from five historical hottest days in July 2022. Profiles for three areas are shown separately.

To address this limitation, we apply a "morphing" approach to artificially create future heatwaves based upon historical weather observations [34, 35]. This approach preserves the spatial structure and diurnal patterns of historical heatwaves while shifting the temperature baseline, though it assumes that heatwave dynamics will remain qualitatively similar under future climate conditions. This approach has often been used for the analysis of building energy use or assessing resilience under different future climate scenarios [36].

We first select temperature profiles from historical heatwave events in the hourly ERA5 reanalysis dataset, denoted as $T^{\text{his}}_{\text{heat}}$, and the historical reference temperature data, $T^{\text{his}}_{\text{ref}}$, on the same historical date. To derive the projected future hourly heatwave scenarios $T^{\text{fut}}_{\text{heat}}$ from the future reference temperature $T^{\text{fut}}_{\text{ref}}$, we calculate it as

$T^{\text{fut}}_{\text{heat}} = T^{\text{fut}}_{\text{ref}} + (T^{\text{his}}_{\text{heat}} - T^{\text{his}}_{\text{ref}})$, where the low-resolution 3-hourly reference data is linearly interpolated to generate a complete 24-hour time series for this calculation.

The projected future heatwave exhibits a similar temperature increase relative to the historical reference (Fig 7a) while preserving the spatial features at each longitude-latitude grid (Fig 7b). Furthermore, we collect a set of such bias values (i.e., $(T^{\text{his}}_{\text{heat}} - T^{\text{his}}_{\text{ref}})$) based on different historical heatwave records, to represent a historical distribution of extreme weather patterns (Fig 7c). This approach allows us to capture the diversity of potential heatwave manifestations while maintaining their inherent spatial characteristics in our future projections.

1.2 Future Demand Modeling

We employ a weather-dependent demand model following Demand.ninja [32] to simulate future daily demand as follows:

$$P^d = P_{\text{base}} + P_{\text{heat}}[T_{\text{heat}} - \text{BAIT}]^+ + P_{\text{cool}}[\text{BAIT} - T_{\text{cool}}]^+ + \alpha W + \beta D + \epsilon,$$

where base load P_{base} denotes the base demand (in GW), P_{heat} and P_{cool} are heating and cooling coefficients (in $GW/°C$), T_{heat} and T_{cool} are heating and cooling thresholds (in $°C$), and BAIT denotes the building-adjusted internal temperature derived from [32], which depends on specific weather conditions such as air temperature, relative humidity, wind speed, and solar radiation. α is a time-dependent coefficient (in GW), representing the impacts of differences in workdays ($W = 1$) and weekends ($W = 0$), β (in GW/yr) captures the long-term yearly trends in power demand, and ϵ is the model error term. After generating daily power demand, we convert it to an hourly resolution based on the historical average hourly demand ratios observed during hot days, following [32].

We follow the methodology [32] to calibrate demand models for EU countries in our case study. For future scenarios, we incorporate varying annual growth rates (β) from 1% to 3% to model different load projections. This approach accounts for unprecedented grid challenges from AI technologies, smart homes, and electric vehicles, which will significantly alter historical demand patterns [23, 24]. By adjusting these growth rates, we evaluate grid performance under various electrification scenarios, from moderate to aggressive technology adoption.

1.3 Generator Derating Modeling

Heatwave-induced high temperatures also derate generator capacity. For renewable generators, such as solar generation, the Atlite package [33] is employed to convert weather data into renewable power generation profiles. For Gas Turbines (GT) and Combined-Cycle Gas Turbines (CCGT), the density of input air decreases with increasing ambient temperature, resulting in more fuel needed to compress the same amount of air mass [14]. Nuclear power generators experience capacity decreases at high temperatures due to their reliance on water cooling systems to prevent overheating [37]. For Electric Generators with copper windings, elevated temperatures increase winding resistance, inducing Joule heating and reducing efficiency [38]. We then summarize the capacity derating factor $\eta \leq 1$ for some conventional generators under

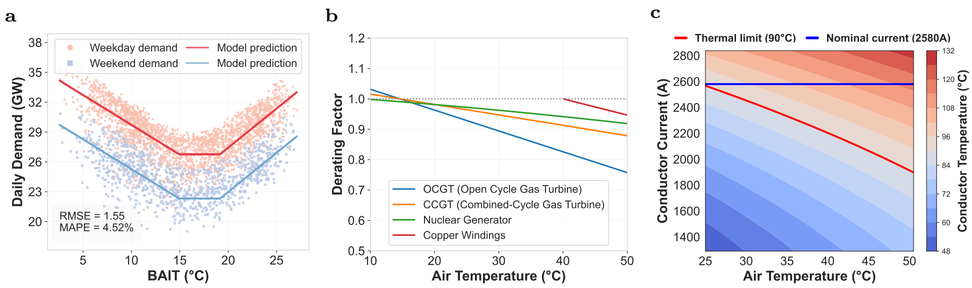

Fig. 8: **Heatwave impacts on load demand, generator efficiency, and transmission capacity. a** Calibrated temperature-dependent demand model for Spain following Demand.ninja [32], where BAIT indicates building-adjusted internal temperature depending on multiple weather variables. **b** Generator derating model for various common generators, where higher ambient temperature induces lower generation efficiency due to different mechanisms. **c** Conductor thermal models based on heat balance equations, where the nominal current capacity is determined under thermal limits in ambient conditions; as air temperature increases, the current limits decrease.

---

ambient temperatures T_{amb} using:

$$\text{Generator derating} \quad \eta = \begin{cases} (-0.6854T_{\text{amb}} + 110)/100 & \text{(GT)} \\ (-0.3427T_{\text{amb}} + 105)/100 & \text{(CCGT)} \\ (101.3042–0.1387T_{\text{amb}}–0.0010T_{\text{amb}}^2)/100 & \text{(Nuclear)} \\ \sqrt{\frac{(180-T_{\text{amb}})[1+0.0039(40-20)]}{(180-40)[1+0.0039(\ T_{\text{amb}}-20)]}}\ (\forall T_{\text{amb}} \geq 40) & \text{(Copper windings)} \end{cases}$$

These coefficients of derating curves depend on the detailed manufacturing configurations of different generators and can be adjusted under different real-world systems [14, 37, 38].

1.4 Conductor Thermal Modeling

Heatwaves also reduce transmission capacity in power grids by affecting the thermal behavior of overhead conductors. This physical phenomenon can be modeled by the steady-state heat balance equation, which accounts for the equilibrium between heat generated by electrical current and solar radiation, and heat lost through convection, radiation, and conduction.

Heat Balance Equations

The standard steady-state heat balance equation according to IEEE Std 738$^{\text{TM}}$-2012 [1] used in our study is as follows:

$$\underbrace{H_C + H_R}_{\text{heat loss}} = \underbrace{H_S + H_J}_{\text{heat gain}} \quad [\text{W/m}], \tag{1}$$

where

$$H_C = \max \begin{cases} 3.645\rho_f^{0.5} D^{0.75} (T - T_{\text{amb}})^{1.25}, & \text{(zero wind speed)}; \\ K_\phi \left[1.01 + 1.35N_{\text{Re}}^{0.52}\right] \lambda_f (T - T_{\text{amb}}), & \text{(low wind speed)}; \\ 0.754K_\phi N_{\text{Re}}^{0.6} \lambda_f (T - T_{\text{amb}}), & \text{(high wind speed)}; \end{cases}$$

$$H_R = \pi\sigma_B D\alpha_{\text{emi}}\left[(T+273)^4 - (T_{\text{amb}}+273)^4\right]$$
$$H_S = \alpha_{\text{abs}} DS$$
$$H_J = I^2 R(T) = I^2 R_{\text{ref}}(1+\alpha_r(T-T_{\text{ref}}))$$

Here, given the conductor physical properties (conductor diameter D, emissivity factor α_{emi}, absorptivity factor α_{abs}, resistance coefficient α_r, unit reference resistance R_{ref}) and environmental variables (conductor temperature T, ambient temperature T_{amb}, air density ρ_f, air thermal conductivity λ_f, wind angle factor K_ϕ, Reynolds number N_{Re}, solar radiation S, and constant δ_B), the heat balance equation solves for the equilibrium conductor temperature that balances heat inflow and outflow. The heat transfer components include convective heat loss H_C, radiative heat loss H_R driven by temperature difference, solar heat gain H_S, and Joule heat gain H_J from conductor current I and temperature-dependent unit resistance $R(T)$. Detailed parameter definitions are provided in Supplementary Table 7.

For simplicity, we denote the implicit mapping from conductor current to equilibrium conductor temperature as $T = \mathcal{H}(I, \mathcal{W})$, where $\mathcal{W}$ includes all environmental variables shown above, such as air temperature and wind speed. We remark that the mapping from current to equilibrium temperature is a single-variable monotonic mapping, i.e., higher current leads to higher conductor temperature given identical weather variables. Thus, it can be efficiently solved using the bisection or Newton's method.

Multi-Bundle Modeling

In practice, multi-bundle transmission lines are commonly used for high-voltage transmission grids, which complicates thermal modeling due to mutual interactions between conductor bundles. Conductors within a bundle experience reduced cooling when positioned in the wake of neighbors, with finite-element simulations showing temperature variations of 5–25℃ between individual bundles in common four-bundle transmission lines [39]. Two simplified modeling approaches are commonly used. Individual conductor modeling treats each bundle independently, overestimating capacity by neglecting mutual thermal shielding [18]. Merged conductor modeling combines bundles into a single equivalent line, underestimating capacity by ignoring inter-bundle convective cooling.

Following finite-element analysis results showing 5–25℃ temperature elevations in shielded conductors within four-bundle configurations [39], we apply a reduction factor of 0.8 to convective and radiative cooling terms as $0.8(H_C + H_R) = H_S + H_J$. Specifically, under worst-case ambient conditions (0.6 m/s wind, 900 W/m^2 solar irradiance) [40], this predicts the 90℃ thermal limit at 25℃ ambient temperature, falling between the two simplified approaches with approximately 15℃ difference from the optimistic individual conductor model, consistent with finite-element simulations showing temperature variations of 5–25℃ [39]. This approximation captures inter-bundle thermal shielding effects without requiring computationally expensive finite-element simulations for each line segment.

Multi-Segment Modeling

Heatwaves further induce spatially heterogeneous effects on grid transmission capacity, especially for long-distance transmission lines. To capture these varied impacts, we compute the intersection of transmission lines with grid lines embedded in weather datasets such as ERA5 (see Fig. 1b). Segments within a single grid cell share the power flow and current, but have different resistances due to thermal effects under various local weather conditions, such as wind speed and solar radiation. For each link, the multi-segment model satisfies the following equations:

$$\text{Heat balance equations} \quad T_{l,s} = \mathcal{H}(I_l, \mathcal{W}_{l,s}),\ \forall s \in \mathcal{S}_l \tag{2}$$

$$\text{Conductor thermal limits} \quad T_{l,s} \leq T^{\max},\ \forall s \in \mathcal{S}_l \tag{3}$$

$$\text{Transimision line resistance} \quad R_l = \sum_{s \in \mathcal{S}_l} d_{l,s} \cdot R(T_{l,s}), \tag{4}$$

The conductor temperature for each segment $s \in \mathcal{S}_l$ from line l in Equation (2) is derived from the heat balance equation (Equations (1)) based on local weather conditions. Segment temperature $T_{l,s}$ is constrained by the transmission line's thermal limit $T^{\max}$ (e.g., 90℃ for ACSR conductors) in Equation (3). The total line resistance equals the sum of segment resistances as shown in Equation (4), where $d_{l,s}$ is the segment's length and $R(T)$ is the temperature-dependent unit resistance. Consequently, branch flow is limited by the segment with the highest temperature. This approach is compatible with any gridded weather dataset, allowing our segmented transmission model to automatically improve in accuracy as weather data becomes more fine-grained.

The comprehensive formulations and discussions for the above thermal models are included in Supplementary Section 3.4, and sensitivity analysis on different conductor physical models is included in Supplementary Section 4.

1.5 Optimal Power Flow Analysis

The Optimal Power Flow (OPF) problem is a fundamental component in electricity grid operations and vulnerability analysis. It aims to determine the most efficient operating conditions for an electrical power system, ensuring that power generation meets the demand while minimizing operational costs and adhering to system constraints.

For different planning horizons, power grid optimization can be categorized into three types: (1) planning problem, which addresses long-term infrastructure development decisions over years to decades; (2) short-term set-point dispatching, which focuses on day-ahead to hour-ahead scheduling of generation resources; and (3) real-time control, which manages immediate system adjustments within minutes to maintain stability and reliability. Each timescale presents distinct objectives, constraints, and computational requirements while sharing the fundamental goal of optimal resource allocation.

In the context of grid vulnerability analysis, we employ hourly single-snapshot OPF simulations to systematically identify grid bottlenecks during extreme weather events. By solving the OPF problem at each hour during extreme periods, we can pinpoint transmission lines, generators, and other components that consistently reach their operational limits, representing critical vulnerabilities in the system. This temporal granularity allows us to capture the dynamic nature of both electricity demand patterns and environmental impacts, particularly during heatwaves when thermal constraints become increasingly binding.

We first introduce the standard single-snapshot alternating-current OPF (AC-OPF) problem in Sec. 1.5 and extend to include conductor thermal modeling in Sec. 1.5, contingency security constraints in Sec. 1.5, and optimization with storage units in Sec. 1.5.

Baseline OPF Methods. To our knowledge, the most standard OPF formulation based on the Alternating Current (AC) model is AC Optimal Power Flow (AC-OPF) [41]. It is a non-linear, constrained optimization problem that incorporates both the physical laws governing power flow and the operational limits of the grid components. Given hourly load demand $\{\boldsymbol{P}^d, \boldsymbol{Q}^d\}$ and grid parameters, we solve the power generation $\{\boldsymbol{P}, \boldsymbol{Q}\}$ and complex-form voltage $\{\boldsymbol{V}\}$ as follows:

$$
\begin{aligned}
\textbf{AC-OPF:} \quad & \min \quad \sum_{i \in \mathcal{N}} \sum_{k \in \mathcal{G}_i} c_{i,k} \cdot P_{i,k}, && (5)\\
& \text{s.t.} \\
\text{Power flow balance} \quad & \begin{cases} \sum_{k \in \mathcal{G}_i} P_{i,k} - P_i^d = \operatorname{re}\left(V_i (\sum_{j \in \mathcal{N}} Y_{ij} V_j)^*\right) \\ \sum_{k \in \mathcal{G}_i} Q_{i,k} - Q_i^d = \operatorname{im}\left(V_i (\sum_{j \in \mathcal{N}} Y_{ij} V_j)^*\right) \end{cases}, \ \forall i \in \mathcal{N}, && (6)\\
\text{Line power flow limits} \quad & |V_i \left((V_i - V_j) \, Y_{ij} \right)^* | \leq S_{ij}^{\max}, \ \forall (i,j) \in \mathcal{L}, && (7)\\
\text{Generations limits} \quad & P_{i,k} \in [P_{i,k}^{\min}, P_{i,k}^{\max}], Q_{i,k} \in [Q_{i,k}^{\min}, Q_{i,k}^{\max}], \ \forall i \in \mathcal{N}, \ \forall k \in \mathcal{G}_i, && (8)\\
\text{Voltage limits} \quad & |V_i| \in [V_m^{\min}, V_m^{\max}], \ |\angle V_{ij}| \leq V_a^{\max}, \ \forall i \in \mathcal{N}, \ \forall (i,j) \in \mathcal{L}, && (9)\\
\text{var.} \quad & \boldsymbol{P}, \boldsymbol{Q}, \ \text{and } \boldsymbol{V}.
\end{aligned}
$$

The objective function in (5) represents total generation cost, calculated as a linear function of power generation and individual generator costs ($c_{i,k}$). The non-linear power flow balance constraints in (6) ensure power injection and load are balanced at each bus, where Y_{ij} is the transmission line admittance. The line flow limits ($S_{ij}^{\max}$) in (7) enforce thermal limits of transmission lines under static conditions. Operating limits for power generation ($P_{i,k}^{\min}, P_{i,k}^{\max}, Q_{i,k}^{\min}, Q_{i,k}^{\max}$), voltage magnitude ($V_m^{\min}, V_m^{\max}$), and voltage angles ($V_a^{\max}$) are specified in (8)–(9).

Compared with Linear or DC-OPF formulations [27], which neglect temperature-dependent resistance and Joule heating losses in transmission lines, AC-OPF more accurately captures the physical behavior of power transmission systems [42] and enables the incorporation of heat flow analysis.

OPF under Heatwaves. Standard AC-OPF neither incorporates the impact of weather on the electrical network's parameters, such as resistance, nor the dynamic thermal limits of transmission lines. Temperature-Dependent AC Optimal Power Flow (TD-OPF) [16, 42, 43] extends it by incorporating heat flow equations and temperature constraints in Sec. 1.4. AC-based TD-OPF is formulated as follows:

$$
\begin{aligned}
\textbf{TD-OPF:} \quad & \min \quad (5) \\
& \text{s.t.} \\
\text{ACOPF constraints} \quad & (6) - (9), \\
\text{Heat flow constraints} \quad & (2) - (4), \ \forall l = (i,j) \in \mathcal{L}, \\
\text{Line current flow} \quad & I_l = |(V_i - V_j) Y_{ij}|, \ \forall l = (i,j) \in \mathcal{L}, && (10)\\
\text{Line admittance} \quad & Y_l = 1/(R_l + \mathrm{i} \cdot X_l), \ \forall l = (i,j) \in \mathcal{L}, && (11)
\end{aligned}
$$

$$\text{var.} \quad \boldsymbol{P}, \boldsymbol{Q}, \text{ and } \boldsymbol{V}.$$

In this formulation, standard AC-OPF constraints and heat flow constraints are coupled through line current magnitude in (10) and temperature-dependent line admittance in (11), where R_l is the line resistance and X_l is the line reactance. The current flow generates Joule heating H_J, which increases conductor temperatures. The constraints from (2) to (4) model heat transfer in individual transmission line segments under varying local weather conditions, ensuring permissible steady-state conductor temperatures that determine line current-carrying capacities. The interdependence of electrical and thermal constraints in the TD-OPF model more accurately captures physical grid behavior than linearized models during heatwaves.

Load Shedding Analysis. We implement all operational constraints as hard constraints in our optimization formulation, ensuring that transmission line flows cannot exceed the specified limits. To assess grid bottlenecks under safety operation conditions, we introduce slack variables representing load shedding in the power balance equations and add a large penalty term for load shedding in the objective function. This approach allows the model to identify when and where the grid cannot meet demand while respecting security constraints, providing quantitative measures of grid vulnerability during heatwave events.

Security Contingency Analysis. Beyond modeling weather-induced thermal limits in AC-based TD-OPF, N-1 security constraints are widely implemented to enhance grid operation robustness by ensuring system stability following any single line outage [44]. These constraints require that all operational limits remain satisfied in both the base case and all post-contingency states. The base case and post-contingency states are coupled through generator ramping constraints: preventive formulations fix real power generation dispatch across all states, while corrective formulations permit decision variables to adjust within prescribed ranges following contingency occurrence.

Computational complexity scales linearly with the number of contingencies, motivating research into simplified security constraint formulations. Two common approaches prevail in the literature. The first applies a fixed percentage reduction (e.g., 70%) to thermal limits within AC-OPF models, establishing implicit safety margins without explicit contingency enumeration [18, 27]. The second integrates linearized security constraints based on Line Outage Distribution Factors (LODFs) to approximate contingency impacts within DC-OPF frameworks [45].

We adopt different approaches depending on system scale and data availability. For the IEEE 30-bus test system (Supplementary Section 5), we implement standard N-1 preventive security-constrained AC-OPF under heatwave conditions, leveraging its complete topology and system parameters while maintaining computational feasibility. For larger-scale European country-level analysis, we adopt the established 70% fixed security margin approach from PyPSA-Eur [27]. This choice reflects two practical constraints: network clustering introduces an incomplete topology that precludes rigorous contingency definition, and explicit contingency modeling at a continental scale imposes a prohibitive computational burden for AC-based formulations.

Impact of Storage and State of Charge. The expanding deployment of distributed energy storage offers potential for mitigating local capacity constraints and absorbing renewable generation variability through strategic charging and discharging. However, directly incorporating these temporal dynamics into AC-based TD-OPF presents significant methodological challenges: Solutions become dependent on state-of-charge initialization, require extended time horizons spanning days to years to capture storage behavior under variable weather conditions, and substantially increase computational complexity.

To balance analytical rigor with computational tractability, we adopt a simplified approach. Using existing storage infrastructure configurations from PyPSA-Eur-derived grid data (see Supplementary Table 5 for details), we implement a baseline scenario assuming 80% initial state of charge. This value reflects typical operational practices wherein grid operators pre-charge storage assets ahead of anticipated high-demand periods to ensure sufficient reserve margins [46]. We further complement this baseline with comprehensive sensitivity analyses across the full range of storage states (0–100%) to characterize how storage availability affects system vulnerability. Results show that even at 100% state of charge, storage provides only marginal relief from load shedding (Fig. 4d), indicating that transmission constraints—not storage capacity—dominate grid vulnerability during extreme heat. Under this framework, storage units function as dispatchable generators in our single-snapshot analysis of extreme heatwave conditions.

1.6 Algorithm Design

For standard AC-OPF, Interior Point Methods (IPMs) have demonstrated effectiveness across various IEEE test scenarios [28, 47]. Extending these methods to solve AC-based TD-OPF markedly increases complexity due to the interdependence of electrical and thermal constraints.

Existing Algorithms

Existing studies adopt different approximation methods to solve AC-based TD-OPF

- Linear approximation (DC-OPF and TD-DC-OPF): This approach linearizes the nonlinear constraints in AC-OPF and incorporates weather-dependent dynamic line ratings [15, 16, 48]. However, it generally overlooks the interactions between heat flow and power flow, leading to substantial inaccuracies in the resolved power flows.
- Quadratic approximation (Quad-OPF): It uses a quadratic function to estimate steady-state conductor temperature [17], expressed as $T_c \approx \beta_0 + \beta_1 I^2 + \beta_2 I^4$ with weather-dependent coefficients $\{\beta_0, \beta_1, \beta_2\}$. This simplified version of the heat balance equation is then integrated into the standard AC-OPF model.

While these approximations enhance computational efficiency, they often fail to fully satisfy physical constraints on heat and power balance equations, particularly under stringent temperature-induced thermal constraints. These methods frequently overlook potential capacity constraints, resulting in inaccuracies when evaluating grid performance under extreme weather scenarios.

Algorithm 1 Iter-OPF Analysis

Data: Weather data, conductor thermal model, and power grid model.
Result: Grid operational states under heatwaves.

For each segment, given the gridded weather data, transform the temperature limit to the current constraint as Equation (12).
For each line, select the minimum current limit among segments as the line current constraint as Equation (13).
while *conductor temperature not converge* **do**
  Update temperature-dependent admittance for every segment as Equation (11).
  Aggregate segment admittance into line admittance as Equation (4).
  Solve AC-OPF with updated admittance and current constraints (13) via IPOPT.
  Update the line current derived from the OPF analysis as Equation (10).
  Solve heat flow equations in (1) for all segments via Bisection methods.
  Update the segment temperature derived from heat flow equations.
end

Despite these advancements, developing an efficient algorithm capable of solving AC-based TD-OPF models while satisfying all physical constraints has been a significant gap that we address in this work.

Proposed Iterative Analysis (Iter-OPF)

In this work, we propose a novel iterative framework for efficiently solving AC-based TD-OPF. As illustrated in Figure 2b and detailed in Algorithm 1, this algorithm employs two key steps that improve computational efficiency and solution accuracy.

- First, we convert steady-state conductor temperature constraints into equivalent conductor current constraints based on local segment weather conditions [15, 48]:

$$I_{l,s}^{\max} = \sqrt{(H_C + H_R - H_S)/(R(T^{\max}))},\ \forall l = (i,j) \in \mathcal{L},\ \forall s \in \mathcal{S}_l \tag{12}$$

$$I_l = |(V_i - V_j)Y_{ij}| \leq \min_{s \in \mathcal{S}_l}\{I_{l,s}^{\max}\},\ \forall l = (i,j) \in \mathcal{L} \tag{13}$$

  This strictly enforces line thermal limits under temperature conditions while eliminating explicit steady-state temperature expressions, effectively decoupling heat and power balance equations.
- inspired by decoupling approaches for TD power flow equations [42, 49], we develop an alternating update mechanism where (i) AC-OPF is solved with additional current constraints from (13) and (ii) heat balance calculations are conducted in parallel for each segment. Empirical evaluations demonstrate that two iterations are sufficient to achieve results nearly indistinguishable from fully converged solutions, with average errors below 1% for both load shedding and line temperature metrics (Fig. 4). A comprehensive comparison is provided in Supplementary Section 4.

By decoupling heat and power balance constraints, our algorithm enables flexible and precise assessment of grid conditions under diverse thermal and electrical properties. This approach fills a critical gap in OPF studies by efficiently solving AC-based TD-OPF while maintaining physical accuracy, thereby enabling rigorous grid analysis for policy decisions during extreme weather events. As climate variability increasingly threatens grid stability, such tools become essential for utilities to predict and mitigate thermal stress on transmission systems.

European Simulation Overview

To investigate European electricity grid resilience under projected future heatwaves, we integrate grid and weather data using our modeling framework to conduct OPF analysis for Western Europe, with detailed settings in Supplementary Section 3.

We focus on eight Western European countries (Spain, Portugal, France, Italy, Germany, Belgium, the Netherlands, and the UK) impacted by historically recorded heatwaves in 2019 and 2022 (Supplementary Table 3). Using the PyPSA-Eur framework, we derive the power grid configurations detailed in Supplementary Table 4 and Supplementary Table 5.

For network resolution, we adopt a clustered grid that merges nearby buses and lines to mitigate local modeling inaccuracies, such as mis-assignment of loads and under-representation of underground cabling, reducing error-induced bottlenecks [18, 50]. All under-construction lines are included to enhance grid connectivity and provide a more optimistic assessment of capacity under stress. We standardize transmission lines to "Al/St 240/40 4-bundle 380.0" (Aluminium/Steel cross-section 240/40 mm^2, 4-bundle configuration at 380 kV) [18, 51]. Thermal limits are set at 90℃ for Aluminum-type conductors, within the typical 80–120℃ operating range [17, 40, 52–55].

Since PyPSA-Eur data are designed for DC/linear dispatch models, we augment them for OPF simulations. Voltage magnitude is constrained to $0.95 \leq V_m \leq 1.05$ following grid standards [28]. Reactive power demand is set proportional to active power ($Q_d = 0.15 \cdot P_d$) following EnerPol recommendations [56]. We relax other AC-OPF constraints, such as branch phase angle limits, as this information is not available in existing grid profiles [15].

In summary, our model adopts a conservative approach by using an aggregated network topology with relaxed constraints, enabling exploration of upper limits of grid performance and identification of potential bottlenecks under extreme conditions. These insights pinpoint areas requiring more stringent controls under actual operation. Our framework can also incorporate additional constraints with realistic data for more accurate evaluations, as demonstrated by exact solutions for the IEEE 30-bus benchmark (Supplementary Section 5) alongside the EU analysis.

Author contributions

S.K. and M.C. conceived the study. E.L. collected the data for motivation and experiments. E.L., M.C., and S.K. developed the formulation. E.L. developed the algorithm. E.L. conducted the experiments. E.L., M.C., and S.K. analyzed the algorithm performance and experimental results. E.L., M.C., and S.K. wrote and improved the manuscript.

Data availability

The results from the model that support the findings of this study are presented in the main text and Supplementary Information. All data used for validation are publicly available from the sources in Supplementary Table 1.

Code availability

The Iter-OPF algorithm developed in this study is available in the GitHub repository (https://emliang.github.io/Heat-Analysis/). The code is implemented in Python and can be accessed for replication and further research.

References

[1] Ieee standard for calculating the current-temperature relationship of bare overhead conductors. *IEEE Std 738-2012 (Revision of IEEE Std 738-2006 - Incorporates IEEE Std 738-2012 Cor 1-2013)* 1–72 (2013).

[2] IPCC. *Climate Change 2021: The Physical Science Basis. Contribution of Working Group I to the Sixth Assessment Report of the Intergovernmental Panel on Climate Change* (Cambridge University Press, Cambridge, United Kingdom and New York, NY, USA, 2021).

[3] Perkins-Kirkpatrick, S. & Lewis, S. Increasing trends in regional heatwaves. *Nature Communications* **11**, 3357 (2020).

[4] Miranda, N. D. *et al.* Change in cooling degree days with global mean temperature rise increasing from 1.5° c to 2.0° c. *Nature Sustainability* **6**, 1326–1330 (2023).

[5] Vautard, R. *et al.* Heat extremes in western europe increasing faster than simulated due to atmospheric circulation trends. *Nature Communications* **14**, 6803 (2023).

[6] Ballester, J. *et al.* Heat-related mortality in europe during the summer of 2022. *Nature medicine* **29**, 1857–1866 (2023).

[7] Gallo, E. *et al.* Heat-related mortality in europe during 2023 and the role of adaptation in protecting health. *Nature medicine* **30**, 3101–3105 (2024).

[8] Janoš, T. *et al.* Heat-related mortality in europe during 2024 and health emergency forecasting to reduce preventable deaths. *Nature Medicine* **31**, 4065–4074 (2025).

[9] Liu, L. *et al.* Climate change impacts on planned supply–demand match in global wind and solar energy systems. *Nature Energy* **8**, 1–11 (2023).

[10] Sun, Y. *et al.* Global supply chains amplify economic costs of future extreme heat risk. *Nature* **627**, 797–804 (2024).

[11] Dumas, M., Kc, B. & Cunliff, C. I. Extreme weather and climate vulnerabilities of the electric grid: A summary of environmental sensitivity quantification methods. Tech. Rep., Oak Ridge National Lab.(ORNL), Oak Ridge, TN (United States) (2019).

[12] Xu, L. *et al.* Resilience of renewable power systems under climate risks. *Nature Reviews Electrical Engineering* **1**, 53–66 (2024).

[13] You, J., Yin, F. & Gao, L. Escalating wind power shortages during heatwaves. *Communications Earth & Environment* **6**, 245 (2025).

[14] Ke, X., Wu, D., Rice, J., Kintner-Meyer, M. & Lu, N. Quantifying impacts of heat waves on power grid operation. *Applied energy* **183**, 504–512 (2016).

[15] Glaum, P. & Hofmann, F. Leveraging the existing german transmission grid with dynamic line rating. *Applied Energy* **343**, 121199 (2023).

[16] Neumann, F., Hagenmeyer, V. & Brown, T. Assessments of linear power flow and transmission loss approximations in coordinated capacity expansion problems. *Applied Energy* **314**, 118859 (2022).

[17] Ngoko, B. O., Sugihara, H. & Funaki, T. Optimal power flow considering line-conductor temperature limits under high penetration of intermittent renewable energy sources. *International Journal of Electrical Power & Energy Systems* **101**, 255–267 (2018).

[18] Hörsch, J., Hofmann, F., Schlachtberger, D. & Brown, T. Pypsa-eur: An open optimisation model of the european transmission system. *Energy strategy reviews* **22**, 207–215 (2018).

[19] Stone Jr, B. *et al.* How blackouts during heat waves amplify mortality and morbidity risk. *Environmental Science & Technology* **57**, 8245–8255 (2023).

[20] Wu, X. *et al.* Future heat-related mortality in europe driven by compound day-night heatwaves and demographic shifts. *Nature Communications* **16**, 7420 (2025).

[21] Schäfer, B., Witthaut, D., Timme, M. & Latora, V. Dynamically induced cascading failures in power grids. *Nature communications* **9**, 1975 (2018).

[22] Xu, L., Lin, N., Poor, H. V., Xi, D. & Perera, A. Quantifying cascading power outages during climate extremes considering renewable energy integration. *Nature Communications* **16**, 2582 (2025).

[23] Granskog, A., Hernandez Diaz, D. *et al.* The role of power in unlocking the european ai revolution. *McKinsey & Company, October* **24**, 2024 (2024).

[24] Poudineh, R. Global electricity demand: What's driving growth and why it matters (2025).

[25] Buontempo, C. *et al.* The copernicus climate change service: climate science in action. *Bulletin of the American Meteorological Society* **103**, E2669–E2687 (2022).

[26] ENTSO-E. Opportunities for a more efficient European power system by 2050: Infrastructure Gaps Report. Tech. Rep., European Network of Transmission System Operators for Electricity (2025).

[27] Brown, T., Hörsch, J. & Schlachtberger, D. Pypsa: Python for power system analysis. *arXiv preprint arXiv:1707.09913* (2017).

[28] Babaeinejadsarookolaee, S. *et al.* The power grid library for benchmarking ac optimal power flow algorithms. *arXiv preprint arXiv:1908.02788* (2019).

[29] Hersbach, H. *et al.* The era5 global reanalysis. *Quarterly journal of the royal meteorological society* **146**, 1999–2049 (2020).

[30] Copernicus Climate Change Service. Climate and energy indicators for europe from 2005 to 2100 derived from climate projections (2021). URL https://cds.climate.copernicus.eu/datasets/sis-energy-derived-projections?tab=overview. Accessed: 2024-10-06.

[31] Hirth, L., Mühlenpfordt, J. & Bulkeley, M. The entso-e transparency platform–a review of europe's most ambitious electricity data platform. *Applied energy* **225**, 1054–1067 (2018).

[32] Staffell, I., Pfenninger, S. & Johnson, N. A global model of hourly space heating and cooling demand at multiple spatial scales. *Nature Energy* 1–17 (2023).

[33] Hofmann, F., Hampp, J., Neumann, F., Brown, T. & Hörsch, J. Atlite: a lightweight python package for calculating renewable power potentials and time series. *Journal of Open Source Software* **6**, 3294 (2021).

[34] Eames, M., Kershaw, T. & Coley, D. A comparison of future weather created from morphed observed weather and created by a weather generator. *Building and Environment* **56**, 252–264 (2012).

[35] Herrera, M. *et al.* A review of current and future weather data for building simulation. *Building Services Engineering Research and Technology* **38**, 602–627 (2017).

[36] Chan, A. Developing future hourly weather files for studying the impact of climate change on building energy performance in hong kong. *Energy and Buildings* **43**, 2860–2868 (2011).

[37] Linnerud, K., Mideksa, T. K. & Eskeland, G. S. The impact of climate change on nuclear power supply. *The Energy Journal* **32**, 149–168 (2011).

[38] Elsebaay, A., Adma, M. A. A. & Ramadan, M. Analyzing the effect of ambient temperature and loads power factor on electric generator power rating. *International Journal of Energy and Power Engineering* **11**, 171–176 (2017).

[39] Yang, W. *et al.* Thermal analysis for multi-conductor bundle in high voltage overhead transmission lines under the effect of strong wind. *Electric Power Systems Research* **231**, 110308 (2024).

[40] ENTSO-E. Technologies for transmission system. Technical Report, European Network of Transmission System Operators for Electricity (2018). URL https://eepublicdownloads.blob.core.windows.net/public-cdn-container/clean-documents/tyndp-documents/TYNDP2018/consultation/Technical/Technologies4TS.pdf. TYNDP 2018.

[41] Cain, M. B., O'neill, R. P., Castillo, A. *et al.* History of optimal power flow and formulations. *Federal Energy Regulatory Commission* **1**, 1–36 (2012).

[42] Frank, S., Sexauer, J. & Mohagheghi, S. Temperature-dependent power flow. *IEEE Transactions on Power Systems* **28**, 4007–4018 (2013).

[43] Ahmed, A., McFadden, F. J. S. & Rayudu, R. Weather-dependent power flow algorithm for accurate power system analysis under variable weather conditions. *IEEE Transactions on power systems* **34**, 2719–2729 (2019).

[44] Capitanescu, F. *et al.* State-of-the-art, challenges, and future trends in security constrained optimal power flow. *Electric power systems research* **81**, 1731–1741 (2011).

[45] Hörsch, J., Ronellenfitsch, H., Witthaut, D. & Brown, T. Linear optimal power flow using cycle flows. *Electric Power Systems Research* **158**, 126–135 (2018).

[46] Pusceddu, E., Zakeri, B. & Gissey, G. C. Synergies between energy arbitrage and fast frequency response for battery energy storage systems. *Applied Energy* **283**, 116274 (2021).

[47] Kocuk, B. *Global optimization methods for optimal power flow and transmission switching problems in electric power systems.* Ph.D. thesis, Georgia Institute of Technology (2016).

[48] Khaki, M., Musilek, P., Heckenbergerova, J. & Koval, D. *Electric power system cost/loss optimization using dynamic thermal rating and linear programming*, 1–6 (IEEE, 2010).

[49] Ahmed, A., Massier, T., McFadden, F. S. & Rayudu, R. *Weather-dependent ac power flow algorithms*, 1–8 (IEEE, 2020).

[50] Hörsch, J. & Brown, T. *The role of spatial scale in joint optimisations of generation and transmission for european highly renewable scenarios*, 1–7 (IEEE, 2017).

[51] Neumann, F. & Brown, T. *Heuristics for transmission expansion planning in low-carbon energy system models*, 1–8 (IEEE, 2019).

[52] Nigol, O. & Barrett, J. Characteristics of acsr conductors at high temperatures and stresses. *IEEE Transactions on Power Apparatus and Systems* 485–493 (1981).

[53] Douglass, D. & Reding, J. Ieee standard for calculating the current-temperature of bare overhead conductors. *IEEE Standard* 738–2006 (2007).

[54] Abboud, A. W., Gentle, J. P., Parikh, K. & Coffey, J. Sensitivity effects of high temperature overhead conductors to line rating variables. Tech. Rep., Idaho National Lab.(INL), Idaho Falls, ID (United States) (2020).

[55] Ngoko, B., Sugihara, H. & Funaki, T. *A temperature dependent power flow model considering overhead transmission line conductor thermal inertia characteristics*, 1–6 (IEEE, 2019).

[56] Eser, P., Singh, A., Chokani, N. & Abhari, R. S. Effect of increased renewables generation on operation of thermal power plants. *Applied Energy* **164**, 723–732 (2016).